Taylor & Francis
Taylor & Francis Group

Investigation of wind and tidal forcing on stratified flows in Greenland fjords with TELEMAC-3D

Violeta Moloney[a] [ID], Harshinie Karunarathna[a], Tavi Murray[b], Ian Rutt[b], Alistair Everett[b] [ID] and Dominic Reeve[a]

[a]College of Engineering, Swansea University, Swansea, UK; [b]Department of Geography, College of Science, Swansea University, Swansea, UK

ABSTRACT

Many researchers have analysed the effect of wind on fjord dynamics by using two-dimensional numerical models. This paper investigates the wind and tidal forcing effects on the strong stratification and circulation by application of the three-dimensional model TELEMAC-3D. The capability of the model to reproduce the physical processes has been investigated by applying it to Sermilik Fjord, Greenland. This study shows that the major changes in the fjord dynamics are wind induced. Any changes in the wind speed have an instant impact on the water surface velocities. Also, the diffusively driven circulation produced by the horizontal pressure gradients at coast plays an important role in fjord dynamics. After calibration, the tidal model produced matching results with the measured wave height. The tidal analysis shows that the strength and direction of the tidal currents are sensitive to any changes in the width and shape of the domain. The effect of the tidal propagation on the salinity profile has been shown to play an important role, with salinity picks being 5–6 h behind the tidal flood and ebb picks, along the wind forcing, on the fjord circulation. TELEMAC-3D is a suitable model to simulate accurately such complicated dynamics as in presented case study.

1. Introduction

Due to global climate change, retreat of south-east Greenland glaciers has accelerated. As a result, large volumes of freshwater are being added to the fjord domain. Additionally, the frequency of glacier calving events has increased, and such violent occurrences produce more icebergs which terminate in the waters of the North Atlantic Ocean. It is of great importance to study and analyse the current situation, as we need to understand the scale of its impact on the global ocean circulation and what changes it may bring to the future climate of the

---

whole planet. The study area is Sermilik fjord which is located in the south-east part of Greenland. Sermilik fjord is approximately 100 km long, 8 km wide and 600–925 m deep with steep and mountainous coastline (Straneo et al., 2010). Its geographical coordinates are: latitude 65 °N and longitude 38 °W.

The objective of the work presented here was to answer the important questions on which processes have the major impact on the Sermilik Fjord dynamics: What impact the tidal forcing has on the fjord dynamics? Does the wind forcing play a major role on the fjord circulation? Answers to these questions are based on results found from a careful and rigorous application of numerical model.

Observations are sparse, so this affects the quality of the calibration and validation. This paper presents a detailed modelling investigation, using available measurements, to test the existing hypothesis on glacier/fjord/ocean relationship. Some of these tests support existing understanding but some do not, and it is hoped these results will stimulate new field campaigns to gather additional observations.

Many researchers analysed the wind effect on fjord dynamics using two-dimensional numerical models (Klinck, O'Brien, & Svendsen, 1981; Sciascia, Cenedese, Nicoli, Heimbach, & Straneo, 2014). This paper investigates the influence of the wind and tidal forces on the fjord circulation as a whole, by using the three-dimensional non-hydrostatic computational fluid dynamics model TELEMAC-3D.

TELEMAC-3D model is an open-source software that solves hydrodynamic problems using the finite element method on an unstructured triangular grid. The grid is generated by Delaunay finite element method. The code solves the three-dimensional hydrodynamic equations with the following assumptions: three-dimensional non-hydrostatic Navier-Stokes equations and Boussinesq approximation. Various iterative solvers are applied in order to solve the linear systems after discretisation of the equations. For example, the solver of diffusion of velocity is chosen as a conjugate gradient, and for the diffusion of temperature and salinity as conjugate residual methods. Both methods are used to solve the fluid mechanics systems to reach a solution with a minimum number of iterations (Hervouet, 2007).

To ensure the numerical stability by solving the temperature and salinity transport equations, the advection scheme has been set up as an explicit scheme with multidimensional upwind residual distribution. In this case, the stability is conditioned by the value of the Courant number, which should be less than one. The advection of velocity is solved by the method of characteristics that provides unconditional stability where trajectories are calculated by the Runge-Kutta method.

The model runs in parallel on the Swansea University HPC Cluster supercomputer on eight processors, in order to speed up the time of the simulation. Various time steps have been considered: for the wind simulation the 10-sec time step was set up and for the tidal simulation – 60 s. The code is written in Fortran90 and has been run under a Linux operating system. Delft3D-QUICKPLOT, a programme written in MATLAB, has been used to visualise and analyse the simulation results

(http://www.deltaressystems.com). The MATLAB toolbox, *t_tide*, has been used to perform the tidal harmonic analysis of the simulated flow in the fjord (http://www.eos.ubc.ca/~rich/t_tide).

The paper is organised as follows: the model set-up parameters, grid, boundary and initial conditions are presented in Section 2. The results of the numerical simulations of wind and tidal forces applications and some details of the tidal harmonic analysis are presented in Section 3. Finally, the conclusions of presented research and suggestions for the future work are highlighted in Section 4.

2. Computational model set-up

2.1. Model equations and parameters

The main parameters that characterise the state of the fjord water are temperature and salinity. The governing equation that describes the evolution of these parameters in time and space may be written as:

$$\frac{\partial T}{\partial t} + \left(\vec{U} \cdot \overrightarrow{grad} \right) T = \text{div}\left(v_T \overrightarrow{grad}(T) \right) + Q \tag{1}$$

where $\vec{U}$ is fluid velocity, T is a tracer (salinity or temperature), v_T is a tracer diffusion coefficient, t is time and Q is tracer source or sink (Hervouet, 2007).

The wind plays a very important role in the fjord mixing and establishing the circulation (Cottier et al., 2010). The wind forcing is represented in TELEMAC-3D by the following equation:

$$v \frac{\partial \vec{u}_H}{\partial n} = \frac{\rho_{\text{air}}}{\rho} a_{\text{wind}} \vec{W} || \vec{W} || \tag{2}$$

where $\rho_{\text{air}} = 1.29 \text{kg/m}^3$, $\vec{u}_H$ is the horizontal velocity at a surface, $v \frac{\partial \vec{u}_H}{\partial n}$ is stress and $\vec{W}$ is the wind velocity 10 m above the water surface with a_{wind} wind coefficient (Hervouet, 2007).

The coefficient for wind influence, for variations in time but uniform in space, is calculated in the TELEMAC METEO subroutine with application of Equation (2).

The friction coefficient is a very important factor in the model calibration. TELEMAC-3D offers users a choice of four friction laws: Chézy, Strickler, Manning and Nikuradse laws. The friction coefficient depends on the depth. When constant Chézy value is applied, the friction coefficient remains constant with depth, whereas the constant Strickler, Nikuradse or Manning values are applied, the friction coefficients increase with depth decrease. This means the reduction of the near-bed velocities. All available laws with various friction coefficients were tested and compared against data. The best result, with the lowest RMSE (= 0.05 m) for the tidal model, was achieved with the Nikuradse friction law with its bottom and lateral wall coefficients as $K_s = 0.01$. This value has been applied

in all cases presented in this paper. The Nikuradse friction law is implemented in TELEMAC-3D by the following equation:

$$C_d = 2\left[\frac{K}{\log\left(\frac{12h}{K_s}\right)}\right]^2 \tag{3}$$

where C_d is the friction coefficient, K_s is the Nikuradse bed roughness, K is the *VonKármán* constant ($=0.41$) and h is an average water depth.

In a case when the Coriolis force was considered, the Coriolis coefficient was calculated by the following expression $2\omega \sin(\lambda)$, where the Earth's rotational velocity ω is 7.27×10^{-5} *rad/s* and λ is the latitude of the domain. For this case, the λ value was considered as $65°$ to give the Coriolis coefficient as $1.3178 \times 10^{-4}\ s^{-1}$. Dimensional parameters and variables used in presented simulations are shown in Table 1.

The stability in stratification was achieved by the use of the Munk and Anderson damping function that is incorporated into the Mixing Length turbulence model (Hervouet, 2007). Mostly, the flow is laminar with the Re < 2300.

The heat exchange with the atmosphere has been considered in the model set-up. In the model, the heat flux leaving the domain is computed by application of the following equation:

$$\Phi = -\rho C_p v_T \overline{grad(T)} \cdot \vec{n} = -\rho C_p v_T \frac{\partial T}{\partial z} \tag{4}$$

where $C_p = 4.18 J/kg/°C$ and $\vec{n}$ is the perpendicular pointing outwards from the boundary (Hervouet, 2007).

The wind and tidal cases run with the time step set up as 10 and 60 s, and the total numbers of the time steps were 259200 and 129600 respectively.

Table 1. Dimensional parameters and variables used in simulations.

| Dimensions/Parameters	Wind/Tidal simulation
Fjord model full length – L	137.5 km (85.9 km fjord)
Fjord model full width – W	6–12 km fjord (78.1 km open boundary)
Water depth – H_{max}	~920 m
Δx	1–2 km
Δh	25 m (200 m bottom layer)
Δt	10 s/60 s
Number of time steps	259,200/129,600
Number of layers	30
Number of nodes	117,000
Number of elements	217,380
Coriolis force – f	$1.3178 \times 10^{-4} s^{-1}$
Initial value of salinity at surface – S_{s0}	20 psu
Initial value of salinity at bottom – S_{b0}	35 psu
Initial value of temperature at surface – T_{s0}	0.5 °C
Initial value of temperature at bottom – T_{b0}	4.5 °C
Nikuradse bed roughness – K_s	0.01
Atmospheric pressure – p_{atm}	10^5 Pa
Reference density – ρ_{ref} at $T=4$ °C and $S=0$ psu	999.972 kg/m³

2.2. Model grid and bathymetry

After glacier retreat, a narrow and deep U-shape valley with steep sides is left, which is filled in with the mixture of the glacier melt and the coastal sea water. The topography of the fjord is a complex area, especially if there is a presence of a sill. Compared with other fjords, like Storfjorden (Svalbard), Scoresby Sund (Greenland), Sermilik Fjord does not have a sill (Buch, 2002; Murray et al., 2010; Straneo et al., 2010). The fact, that Sermilik is a sill-free fjord, makes it more vulnerable to any changes in adjacent waters, as it allows for direct exchange between the cold and fresh fjord waters and warm and saline North Atlantic waters at a shelf (Cottier et al., 2010).

The Sermilik fjord bathymetric map has been downloaded from the following website: www.helheim-glacier.org. The bathymetry points have been interpolated using the inverse distance algorithm to create a geometry file that was constructed by the use of an open source software *BLUEKENUE*^{TM} (http://www.nrccnrc.gc.ca/eng/solutions/advisory/ blue_kenue_index.html). The inverse interpolation locates the closest source point in each quadrant and performs distance weighted interpolation from these four points. Also, in order to be able to apply the tidal model in later cases, the bathymetry points had to be converted from latitude and longitude coordinates into WGS84 UTM coordinate system. The mesh was constructed on an unstructured triangular grid on horizontal plane, that later was developed vertically into prismatic shape elements with the addition of many horizontal levels in order to create a vertical mesh.

As has been analysed in detail in Burchard & Rennau (2007), total mixing decreases when grid resolution is increased. To maintain computational efficiency without affecting the quality of the results, the z-level vertical mesh was set up with grid size 25 m. The number of horizontal planes is 30, with evenly spaced vertical grid, except for the bottom layer where the vertical grid is 200 m. This has been done in order to save on computational run time, as most of the dynamics occur in the upper part of the water column. The numerical mixing processes are also sensitive to the size of the horizontal grid. Previous research (Burchard & Rennau, 2007; Riemenschneider & Legg, 2007) on numerical mixing experiments, which tested various horizontal resolutions concluded that a good match with physical mixing can be achieved even with resolution Δx = 2 km. Here, the experiments have Δx = 1 km in the fjord, to capture the rapidly varying bed topography (Figure 1), and gradually increased to Δx = 2 km outside of the fjord area, in order to achieve numerical results being close to the physical mixing. The total number of nodes and elements used is 117000 and 217380 respectively. The horizontal grid of the fjord bottom topography is presented in Figure 1, with the deepest area of the fjord (~920 m) that is located at the southern part of the domain. The longitudinal cross section of the vertical mesh is shown in Figure 2.

In order to avoid any unphysical oscillations and to control tracers' fluxes and preserve tracers' mass conservation at the open boundary, due to the coarse mesh,
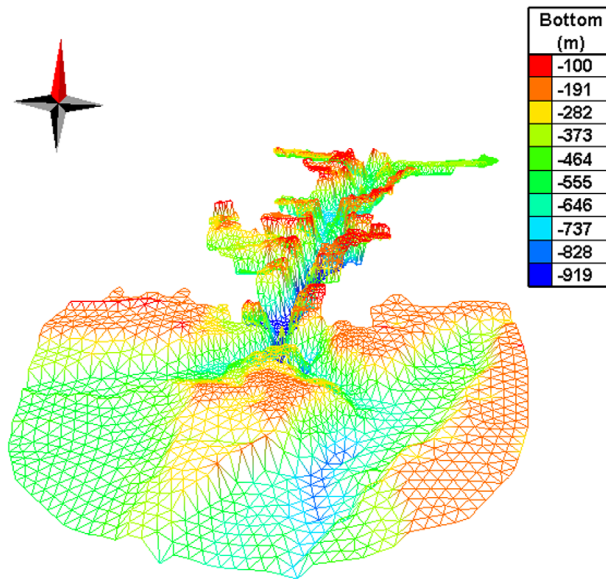
Figure 1. The model horizontal grid of the bottom topography.
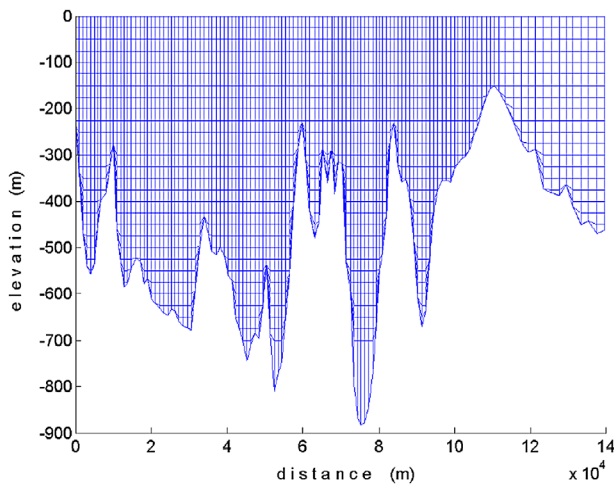
Figure 2. Longitudinal cross section of the vertical mesh.

the Thompson conditions and Multidimensional Upwind Residual Distribution Scheme were set up (see Section 2.3).

2.3. Boundary conditions

Two types of boundaries can be specified in TELEMAC: solid walls and open liquid boundaries. A boundary conditions file was created by the application of previously mentioned software $BLUEKENUE^{TM}$. In this file, the rigid walls (along fjord shores) and one seaward open boundary (fjord mouth) were specified by

assigning requested properties as velocity, tracers' values and water elevation to the specific 2D nodes. These conditions are copied on each vertical level in 3D. In a case of the wind forcing applied on the surface level, the water depth has been prescribed only but no velocities. The non-slip conditions were assigned to the computation of the bottom velocities. The top layer was set up as a free surface level. The constant in time vertical concentration of the salinity and temperature profile that was prescribed at the open boundary can be seen in Figure 3.

In the case of tidal forcing, in order to be able to simulate the tidal propagation in TELEMAC-3D, the tidal current velocity and surface elevation are specified from a global tide model at the open boundary. This model is based on solving the Saint-Venant equations to determine the depth-average tidal flow (Hervouet, 2007). The binary files were downloaded from the TPXO global tidal database that was developed by Oregon State University (http://volkov.oce.orst.edu/tides/). The data from the tidal files are interpolated at the boundary points.

The Thompson conditions have been set up at the open boundary. In a case of not enough information being specified at the open boundary, the Thompson conditions allow one to calculate the missing values, by using the method of characteristics. Also, the treatment of the salinity and temperature fluxes at the open boundary has been set up to give a priority to fluxes, i.e. in order to bring the right mass of the temperature and salinity fluxes passing the open boundary, the prescribed tracers values might be amended.

To ensure the numerical stability by solving the tracer transport equations, the advection scheme has been set up as an explicit scheme with multidimensional upwind residual distribution scheme. In this scheme, the local residuals are distributed to downstream nodes only. For example, if N_0 is an element of the mesh and j is an upstream node of N_0, then coefficient α is zero, i.e. $\alpha_{j,N_0} = 0$. The advantage of the scheme is that it guarantees tracers mass conservation and prevents from the cross-diffusion and unphysical oscillation. In this case, the stability is conditioned by the value of the Courant number, which should be less than 1. The Courant number is computed by the model at every time step. The advection of velocity is solved by the method of characteristics that provides unconditional stability where trajectories are calculated by the Runge-Kutta method (Equation 5) (Hervouet, 2007). With this method, the advection terms of the equation only are taken into account after derivatives in time are discretised. Let the function f represent $h, u, v, k, \varepsilon, T$ and if it is discretised by the fractional step method as $\frac{\tilde{f} - f^n}{\Delta t}$, then the transport-diffusion equation becomes $\frac{\tilde{f} - f^n}{\Delta t} +$ advection terms $= 0$, and in terms of each variable the system of equations is:

$$\frac{\tilde{h} - h^n}{\Delta t} + \vec{u} \cdot \overrightarrow{grad\,(h)} = 0 \,;\, \frac{\tilde{u} - u^n}{\Delta t} + \vec{u} \cdot \overrightarrow{grad\,(u)} = 0 \,;\, \frac{\tilde{v} - v^n}{\Delta t} + \vec{u} \cdot \overrightarrow{grad\,(v)} = 0$$

$$\frac{\tilde{T} - T^n}{\Delta t} + \vec{u} \cdot \overrightarrow{grad\,(T)} = 0 \,;\, \frac{\tilde{k} - k^n}{\Delta t} + \vec{u} \cdot \overrightarrow{grad\,(k)} = 0 \,;\, \frac{\tilde{\varepsilon} - \varepsilon^n}{\Delta t} + \vec{u} \cdot \overrightarrow{grad\,(\varepsilon)} = 0$$
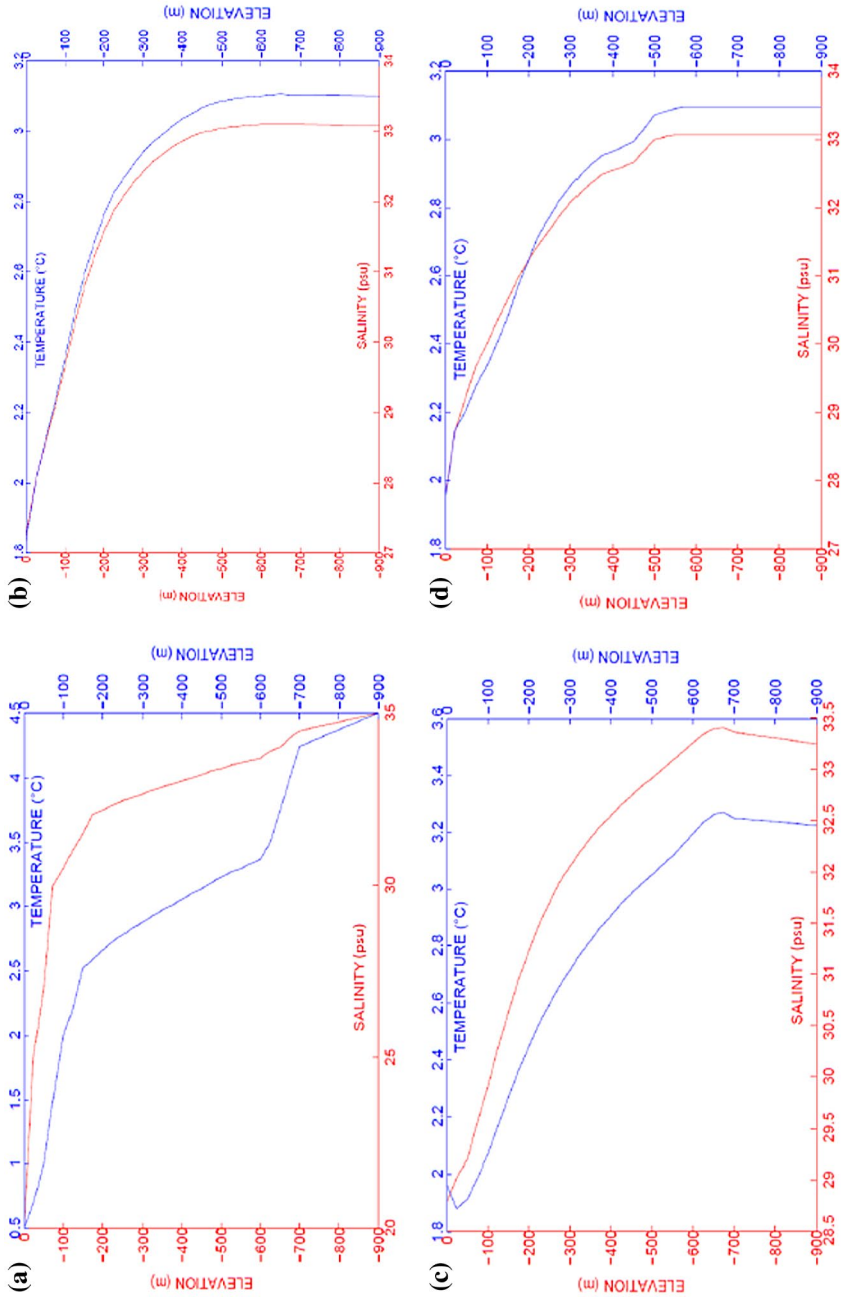
(5)

Figure 3. Temperature and salinity vertical profiles at the first/last time step of the simulation: (a/c) in the middle of the fjord; (b/d) at an open boundary. Temperature values are shown in blue colour and salinity in red.

At these characteristics (trajectories) the total derivative of h, u, etc., is zero and transportation of the quantities along the trajectories stays unchanged. Also, for the model set up the conjugate residual method was chosen to solve for the diffusion terms. This is an iterative method that is used to solve the system of equations. The goal of this method is to define the residual and direction of descent (gradient) that with every new iteration will achieve the minimum for direction of descent (Hervouet, 2007).

2.4. Stratification

One of the main challenges was to create the matching conditions for the tracer profile between the domain and open boundary. The active tracers are temperature and salinity. Initial conditions of temperature was set up 4.5 °C at the bottom of the fjord and at the surface as 0.5 °C, with a logarithmic increase from the top to the bottom on each layer. For salinity, the bottom layer was set up as 35 psu and at the surface as 20 psu, with a gradual increase from top to the bottom in a similar way as for the temperature settings. The values have been adopted from the real observational data for September 2008 published by (Straneo et al., 2010). The initial temperature and salinity vertical profiles in the domain and their prescribed vertical profiles at the open boundary can be viewed in Figure 3(a), (b). Having these water properties set up, and run for one month in model time, without any other forces applied, except the non-linear processes and turbulent mixing, the resulting temperature and salinity profiles were used to prescribe the values at the open boundary. It has been done so in order to avoid the big density differences between domain and open boundary water masses, as water in the fjord would become warmer and more saline with time due to the buoyancy forces effect on shear instabilities between the interfaces, as at the first time step of the simulation, the interfaces are sharp and that would destabilise the Kelvin-Helmholtz mode and would cause the Holmboe instability. The shear instabilities would drive the internal mixing, and as a result the turbulence is generated at the mixing locations. Since the fjord temperature and salinity profiles are mixed after some number of time steps, but at the open boundary the water masses would be still strongly stratified on a constant basis, then as a result of the big density differences between the fjord and the coastal waters, the higher velocities would be triggered in the system due to the large horizontal pressure gradients. The goal was to reach the equilibrium between the fjord and adjacent waters as close as possible. At the end of the simulation (30 days), the values of the temperature and salinity on a vertical scale, at the centre of the domain and at the open boundary, are getting closer and the results are presented in Figure 3(c), (d). The stability was reached on the 7th day of simulations. For this reason the results of the first 10 days are discarded from the results presented in this paper.

3. Results

### 3.1. Wind forcing on fjord circulation

The effect of the wind forcing on the fjord circulation was investigated: firstly, using a constant, uniform wind and secondly, using the measured seasonal winds taken to be uniform over the model domain but time varying.

After 30 days (= 259,200 time steps) of the numerical simulation, the initial tracer values in the fjord have been adjusted due to the double diffusion processes, velocities driven by the density differences between the fjord and coastal waters, and wind forcing. Using the resulting tracers' values, the T-S diagram can be constructed. The T-S diagram with temperature, salinity and isolines of the corresponding density values are presented in Figure 4. The diagram shows the tracers profile on the 30th day of the simulation at a middle point of the fjord. The temperature values plotted against salinity values are shown in blue dotted curve in the diagram. Normally, a linear temperature–salinity relationship indicates the presence of two water masses in the domain. In this case, the non-linear temperature–salinity relationship indicates the presence of more than two water masses with different densities, and hence a multilayer stratified system (Mamayev, 1975). Mainly, in this simulation, the surface layer is a subject of influence of wind and Coriolis forces, but there are also the horizontal pressure gradients due to the constant conditions at the open boundary acting on fjord dynamics.

When alongshore winds are applied, the surface elevation shows the *flooding* or *emptying* results at the head of the fjord, as the Ekman transport pushes water into or out of the fjord, depending on whether the wind direction is westward or eastward. This effect was tested in case of the constant westerly and easterly winds at wind speed 10 m/s. The resulting plots are shown in Figure 5.
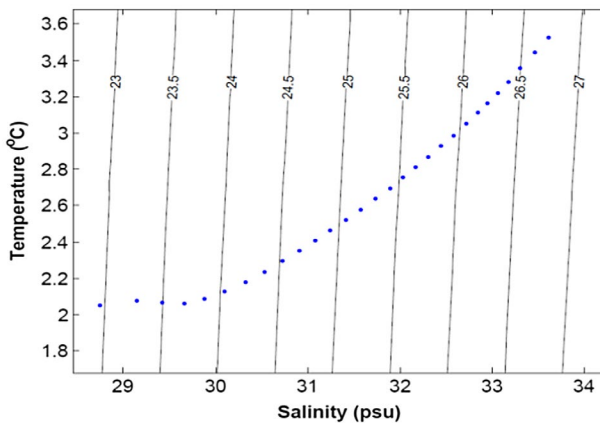

Figure 4. T-S diagram with density isolines at the end of the *August* simulation at a middle fjord point.
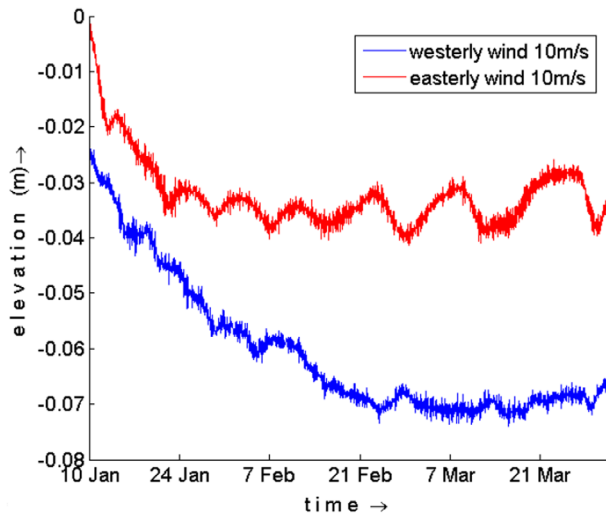
Figure 5. Water surface elevation (in metres) at fjord's head point when westerly 10 m/s wind applied (in blue) and easterly 10 m/s wind (in red).

For the real wind simulation, the *summer* winds firstly, and then the *winter* winds, were applied in a number of independent runs. In both cases, the winds were varied in time: speed and direction, but uniform in space. The real wind data were obtained from the Greenland wind database (www.promice.org) and analysed in detail by Van As, Fausto, Steffen, and PROMICE project team (2014).

The *summer* wind data were used for period of 30 days from 01 to 30 August 2011, and for the *winter* wind period from 01 February to 02 March 2011. The hourly wind data were obtained from the weather station, located on the eastern shore at the fjord mouth, near Tasiilaq (65°24'56" N, 37°29'46" W). The February and August 2011 wind speeds have been plotted in Figure 6. It can be noticed from the graph, that the *winter* winds were much stronger than for *summer* periods.
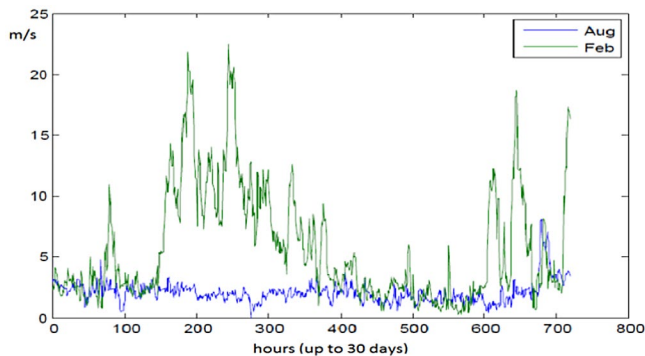

Figure 6. February (in green) and August (in blue) 2011 wind speeds. On the horizontal axis is the number of hours and on the vertical is wind speed (m/s).

This fact has also been mentioned by Jackson, Straneo, & Sutherland, 2014; and other researchers (Sciascia et al., 2014). As data for investigated periods indicate, the wind directions vary, but with dominated north-easterly winds in *winter* and easterly winds in *summer*.

In terms of the February winds, the dominant direction was offshore north-easterly winds and that fact does not change the surface elevation dramatically as net water mass transport is directed partially towards the shoreline. These conclusions are in agreement with those presented by Klinck et al., 1981.

As has been pointed by Cottier et al., 2010; the water surface responds to any wind direction and speed changes instantly. It can be seen in Figure 6, that the wind speed reached the highest value as 22.48/8.11 m/s on 11 February/ 29 August 2011 respectively. Correspondingly, the highest surface velocity magnitude value at a point in the middle of the fjord is 0.8/0.29 m/s, and that occurred on 11 February/29 August 2011 respectively, that is in agreement with the wind velocity fluctuations. The correlation between the wind speed and surface velocity is presented in Figures 7 and 8 for both scenarios. In spite of *summer* wind being slower than *winter*, the 4 m/s wind speed with Coriolis force coupling, sets up the water surface velocity to rise from 0.1 to 0.25 m/s. The surface velocity patterns for periods 18–26 February/August are similar for both scenarios (Figures 7 and 8), with *winter* surface velocity being higher than *summer* velocity by 0.25–0.3 m/s. In both scenarios, the constantly oscillating wind speed varied from 1 m/s to 4 m/s for discussed periods, 18–26 February/August, and this shows that even wind at such speed can drive circulation in the domain.

The long axis of the fjord is north–south, and since the fjord is a long inlet, the longitudinal velocities v (directional velocity along +/-Y axis) are more significant and important in the fjord circulation than the latitudinal velocities u. The isolines
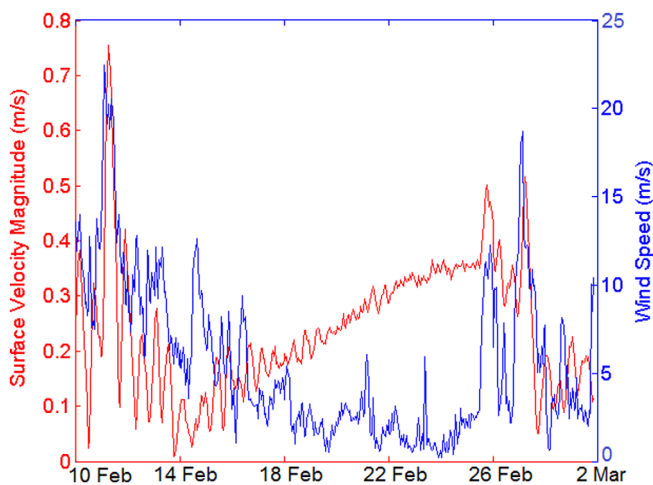

Figure 7. Surface velocity magnitude (in red) at a middle fjord point and wind speed (in blue) for period 10 February–02 March 2011.
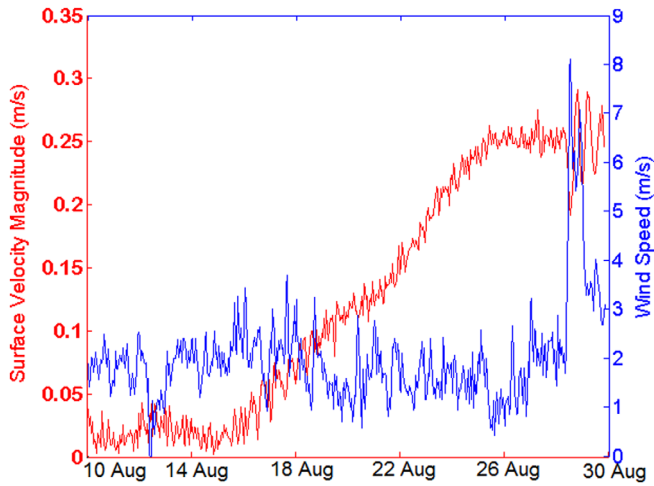
Figure 8. Surface velocity magnitude (in red) at a middle fjord point and wind speed (in blue) for period 10/–30 August 2011.

of the longitudinal velocity of the whole fjord at a surface level (a) and at 100 m below water surface level (b) can be viewed in Figure 9. The northward flow is indicated by the positive values (red colours) in the figure, and the southward by the negative (green colours). Since the velocities are subject to direct wind forcing, their values, through the whole water column, are the highest at the surface level. This statement is applicable in absence of the water discharges in the domain, which is dictated by the source properties: volume of the discharge and its velocity. The vertical velocity magnitude profiles from the results of the numerical

(a) **(b)**
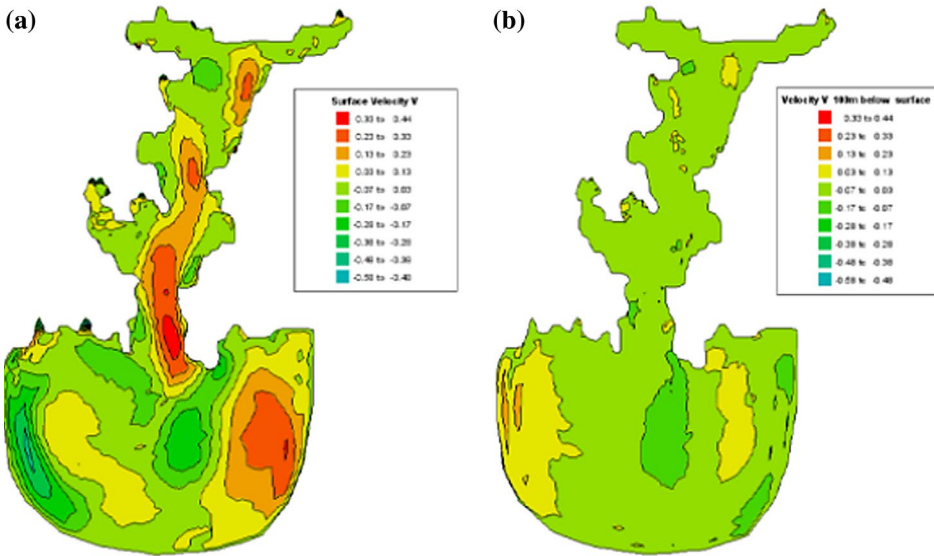
Figure 9. Isolines of the velocity v (longitudinal direction) at the surface level (a) and at 100 m below water surface level at the end of the August simulation.

simulation for both investigated periods are shown in Figure 10. It can be clearly seen in this figure that surface velocities in *winter* period are much higher than in *summer*. The bottom topography at the area from which the middle point vertical velocity profile was extracted, is very deep and narrow with steep mountainous sides (Figure 1). For this reason, to preserve the conservation of mass, the velocity profile is distributed differently in both scenarios, i.e. as domain narrows in this area and due to the stronger winds, the *winter* flow is faster and that affects the velocity at lower parts of the water column as well. Also, the middle point has been taken as an example, but the highest velocity values occurred at various points of the domain, mainly at the eastern side of the fjord entrance, with the highest velocity magnitudes for February being as 1.4 m/s and for August as 0.62 m/s with the velocity decrease below the water surface (Figure 11).

If one compares the results of wind effects on salinity and temperature profiles for both periods, then the differences are not so obvious from first sight. However, if the residue of salinity and temperature values between both scenarios is computed, then it is clearly seen in Figure 12(a), (b), that the water for the summer period is more saline by 0.6 psu in some parts of the surface layer, but fresher by 0.1 psu mostly at the bottom layer than for the winter period at the end of the simulations. Since salinity and heat have different diffusivity rates, i.e. particles loose heat more rapidly than salinity, the temperature contrasts are distributed slightly different: the water for the summer period, nearly through the whole water column, is cooler by 0.01–0.05 °C, but warmer at the surface by 0.2–0.3 °C in comparison with the results for the winter period at the last time step of the simulations (Figure 12(c), (d)). The results present the longitudinal and latitudinal cross sections.
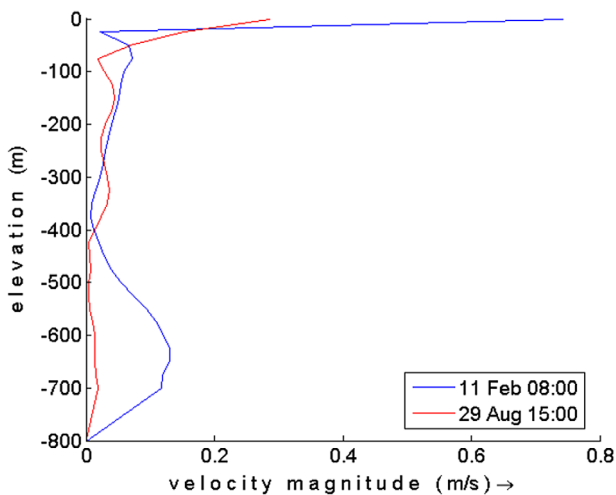
Figure 10. The vertical profiles of the highest velocity magnitude values at a middle of the fjord that occurred on 11 February at 8:00 (in blue) and on 29 August at 15:00 (in red).

Surface velocity vectors (m/s)
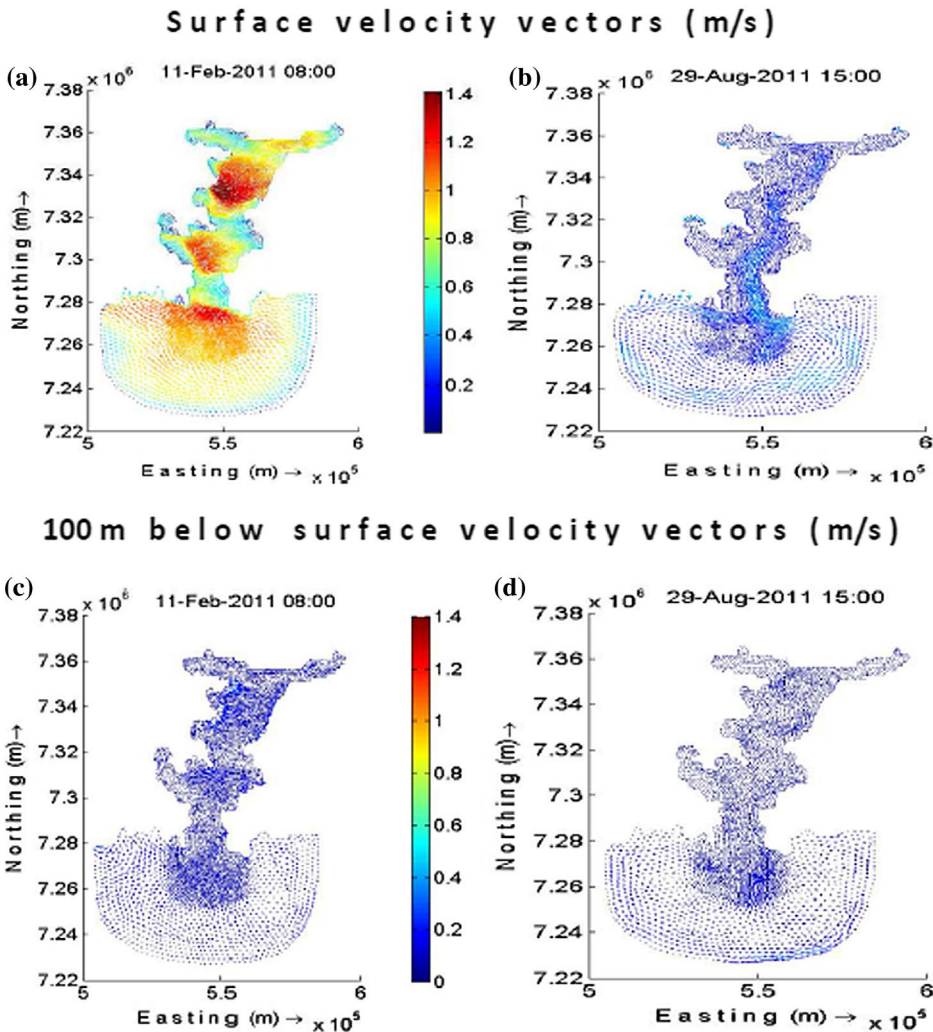
Figure 11. Velocity vectors at their highest values for *winter* and *summer* periods at the surface (a; b) and 100 m below the water surface (c; d).

The wind direction plays an important role in the water mass transport. In spite of the highest values of the surface velocity magnitude for *summer* period still being much lower than for *winter*, it still produced the higher surface elevation. This fact is mostly due to the specific wind directions (Klinck et al., 1981). When alongshore winds are applied the water 'piles up' at the head of the fjord and this was observed in a case of the *summer* wind scenario (Figure 5).

3.2. Tidal forcing on fjord circulation

Tides are the low-frequency waves that are generated by the gravitational attraction between the Earth, the Moon and the Sun (Wells, 1986). When the Moon is
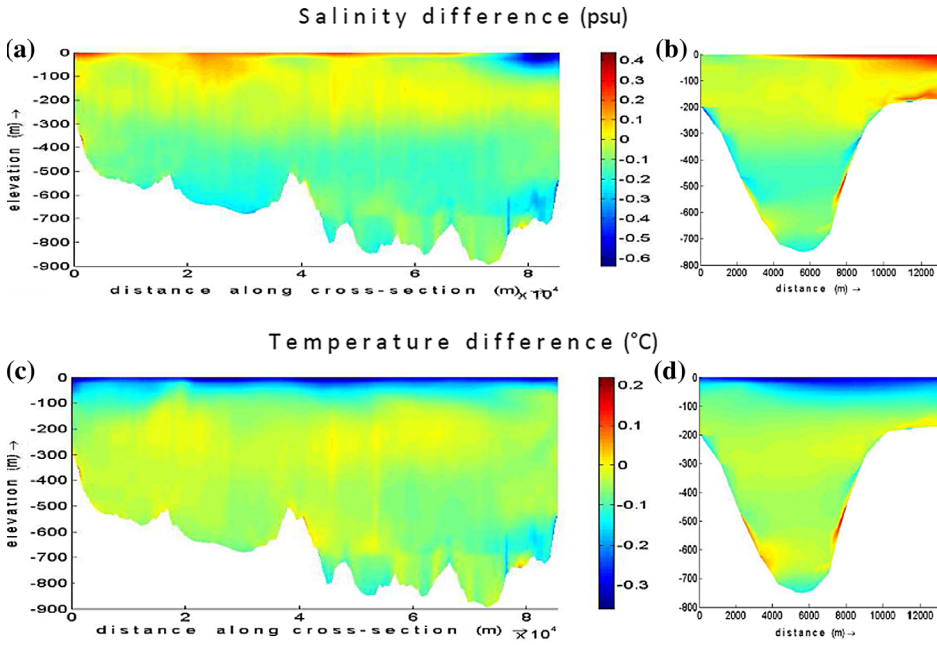
Figure 12. Longitudinal (a;c) and latitudinal (b;d) cross sections of the salinity and temperature values differences between Aug and Feb results at the end of the simulations.

at *zenith*, the gravitational force is greater than centrifugal force, and when the Moon is at *nadir*, then the centrifugal force is greater than gravitational force. The net force F_e is expressed by the formula:

$$F_e = \frac{gm_l}{R^2} \tag{6}$$

where F_e is the net force at the centre of the Earth, g represents the gravity, m_l is the mass of the Moon and R is the distance between the Earth and the Moon.

The tidal force can be calculated by

$$Z_1 = \frac{-2gm_l a}{R^3} \frac{3}{4} \cos\left(2\psi + \frac{1}{3}\right) \tag{7}$$

$$H_1 = \frac{2gm_l a}{R^2} \frac{3}{4} \sin(2\psi) \tag{8}$$

For any point on the Earth surface. The force formula is broken into two components, Z_1 – vertical and H_1 - horizontal, where a is the radius of the Earth and ψ is the angle between the point and the Moon overhead (Wells, 1986).

In the deep ocean, the velocity of tidal currents varies between 1 and 10 cm/s with rise and fall of tides of 10–100 cm in amplitude. However, it was observed that tidal velocities and amplitudes are much greater at a shelf and estuaries than in a deep ocean, with a range of velocity from 1 to 5 m/s and amplitudes of over 10 m. The tidal data from Sermilik fjord shows that the tides are semidiurnal with amplitude in range of 3–5 m.

The following aspects can distort the tidal wave: Corriolis force, water depth and presence of continents (Wells, 1986). All these parameters have been considered in TELEMAC-3D tidal modelling that is described in this paper.

The available fjord tidal data is for the period of 20–23 August 2011 with 7 min data frequency. The pressure measurements were taken by a Sea-Bird MicroCat deployed around 14 m, located in the bay to the west of the island in the upper part of the fjord, at geographical point: latitude 66.178, longitude −37.864. The data was used for the model validation.

The TPXO tidal data were used to specify tidal conditions at the open boundary. This provides the amplitudes and phases of 11 main tidal harmonic constituents (Egbert & Erofeeva, 2002). When the tidal harmonic analysis is performed, the assumption is made that the flood and ebb of the tide is the sum of all harmonics (Schureman, 1941). Tidal harmonic analysis was conducted with the use of MATLAB code – *t_tide* (Pawlowicz, Beardsley, & Lentz, 2002). A comparison of measured and modelled amplitudes of 5 most important tidal constituents is shown in Table 2.

It can be noticed that the most significant constituent is M_2, which has period 12 h 25 min 14 s. Also, the validation results of the tidal simulation against measurements, with RMSE = 0.05 m, are shown in Figure 13. The model tidal amplitude is in good agreement with the data, that is also supported by the small value of RMSE (Equation 9). To calculate the error between numerical simulation results and data, the following formula was used:

$$RMSE = \sqrt{\frac{\sum_{i=1}^{n}(X_i - O_i)^2}{n}} \tag{9}$$

where X_i is the output of the simulation results O_i is measurements and n is the total number of data points analysed. The simulation does not include the wind forcing, when it does, the better match shall be expected.

Velocities of the current flow vary with the water depth. At deeper levels of the water column, the velocities are lower than that at upper levels due to the tidal forcing, Coriolis force and Ekman water mass transport. The residual (mean)

Table 2. Amplitudes (in metres) from the data, model results and their differences.

	M_2	S_2	N_2	K_1	O_1
Data Amp	1.06	0.48	0.21	0.13	0.07
Model Amp	1.08	0.46	0.21	0.13	0.06
Difference	−0.02	0.02	0.00	0.00	0.01
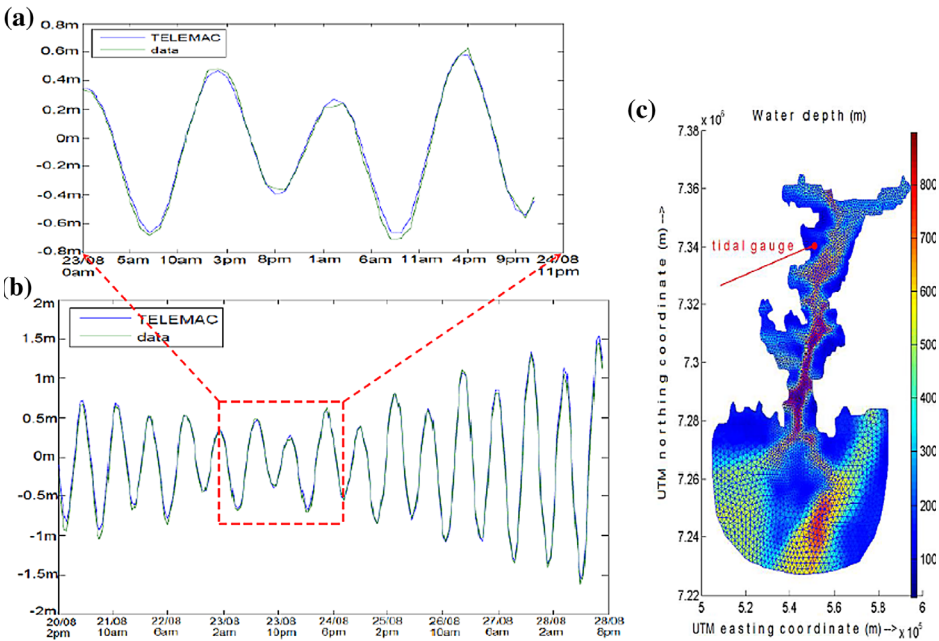
Figure 13. Tidal level TELEMAC-3D and data: (a) two tidal cycles for period 23–24 August 2011; (b) for period 20–28 August 2011; (c) location of a tidal gauge latitude 66.178, longitude −37.864.

flow at a surface level, 50 and 100 m below water surface is calculated from the simulation results for duration of 90 days. The resulting vector plots are shown in Figure 14. As has been pointed by previous researchers (Parker, 2007; Sutherland, Straneo, & Pickart, 2014), the tidal currents increase as they approach the narrower
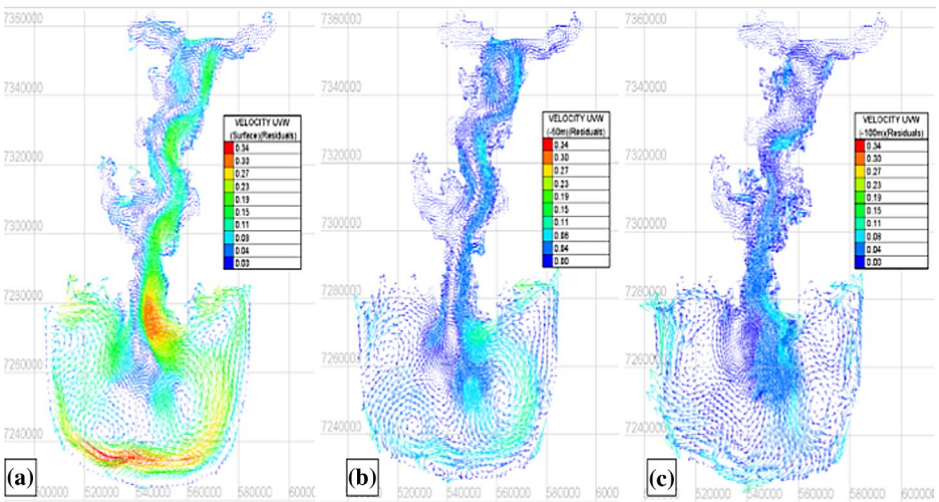
Figure 14. Residual (mean) flows at (a) surface level; (b) 50 m below surface level; (c) 100 m below surface level.

parts of the inlet – domain entrance. The residual flow, extracted from the model results, shows the strongest currents at the entrance to the fjord. As fjord narrows, the same volume of water has to flow through the smaller cross-section area much faster in order to be able to preserve the mass conservation. Also, the curvature and variations in the fjord's width affect the tidal current, as due to the changes in velocities the formation of eddies and whirlpools presents in the fjord (Figure 14(a)).

The tidal energy is dissipated due to friction and as a result it's damping effect on the tidal amplitude. However, when the inlet narrows the velocities increase and friction would play a secondary role. The choice of the bottom and lateral wall friction is very important in the model calibration process. In order to achieve a good match between the tidal amplitudes of the simulation results and data,
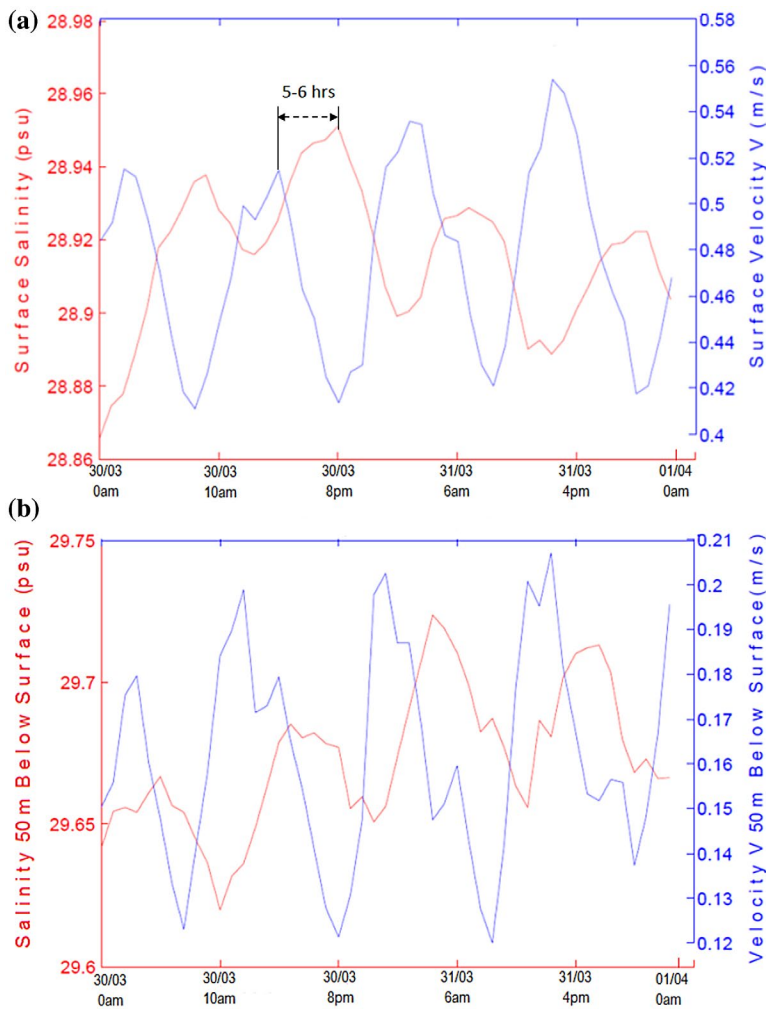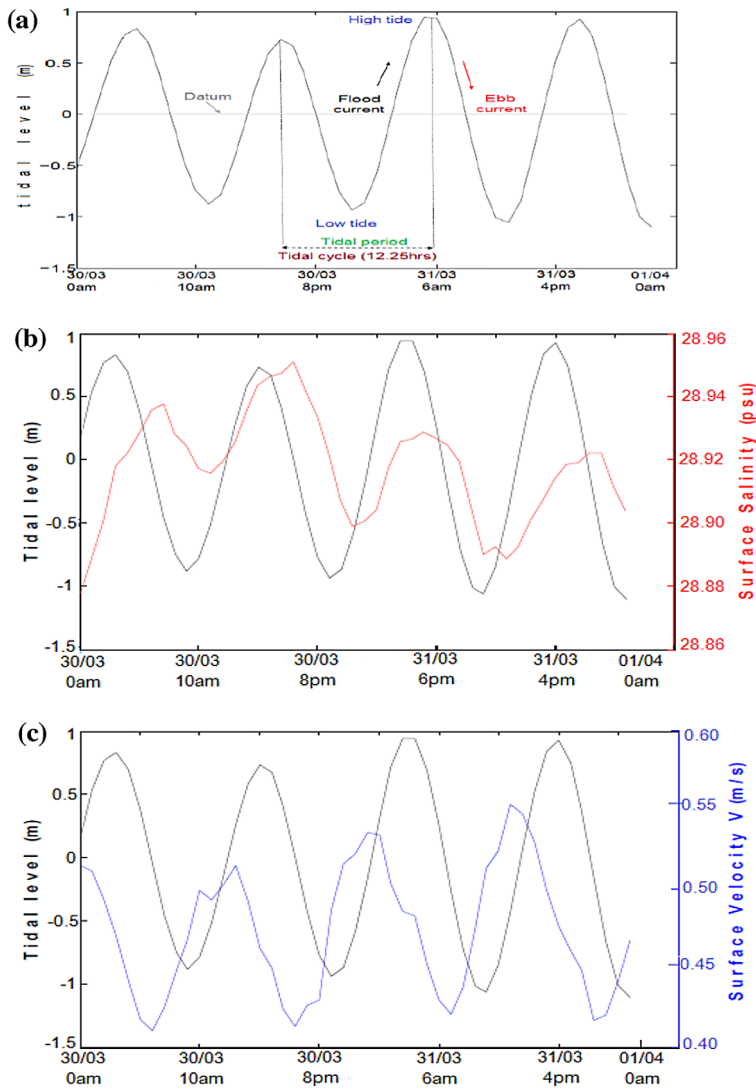

Figure 15. Hourly outputs of salinity and longitudinal velocity at middle of the fjord point at (a) surface level; (b) 50 m below surface level.

various friction laws and their coefficients were tested. As has been mentioned previously, the use of Nikuradse friction law produced best results.

The global tidal database TPXO also stores the history of the tidal amplitudes at various geographical points, so it can be a source for data model results comparisons. The use of the TPXO data, for some points chosen inside of the domain and at an open boundary, produced even lower RMSE = 0.04.

One of the main goals of the tidal modelling in the fjord is to observe how tides affect the stratification at different stages of the tidal propagation through the domain – flood and ebb. Since the fjord is a sill-free inlet, i.e. no barrier

Figure 16. Hourly outputs of: (a) tidal level; (b) salinity and tidal level; (c) longitudinal velocity at the surface and tidal level.

between the coastal and fjord waters, the baroclinic hydraulic jump over the sill is not expected, as it would be in many northern hemisphere fjords, such as LeConte and Columbia fjords (Alaska) (Sutherland et al., 2014). As has been pointed out by previous researchers (McPhee, Skogseth, Nilsen, & Smedsrud, 2013) the salinity picks represent advection that follows the flood and ebb sides of the tidal cycle. The velocities and salinity profiles at the surface level and 50 m below surface level are shown in Figure 15. It can be seen from the figure, how salinity profiles are affected by the tidal current, with approximately 6 h delay: the highest salinity value appears 5–6 h later after the highest tidal velocity values at each tidal cycle. To support the model results, the measurements conducted in Storfjorden (Svalbard) and analysed in details by (McPhee et al., 2013), also show the similar profile of salinity distortion due to the tidal propagation. As can be seen in the figure the salinity decreases with velocity increase, i.e. there is more mixing occurs with increase of the tidal current, as due to the mixing mechanism applied the parcel enters an environment with (greater) less density $\rho' = \rho \pm \Delta\rho$. And contrary, when velocity decreases the salinity raises: the force of the mixing mechanism decreases and particle tries to return to its original position to reach the equilibrium, obeying the Archimedes' force: $= g(\rho' - \rho) = \pm g\Delta\rho$. The flood and ebb parts of the tidal propagation are shown in Figure 16(a). Also the surface salinity and tidal amplitude relationship for duration of two days where an oscillation pattern for both parameters is clearly seen in part (b) of the figure. Both of them are out of phase with salinity picks being behind the high water. The picks of the wave height also fall right at the troughs of the tidal current (c).

The effect of tidal forcing on the vertical and horizontal salinity profile is shown in Figure 17. The figure presents results on the 90th day of the simulation, where clearly can be seen the influence of the prescribed salinity values at the open boundary on the whole fjord salinity profile.
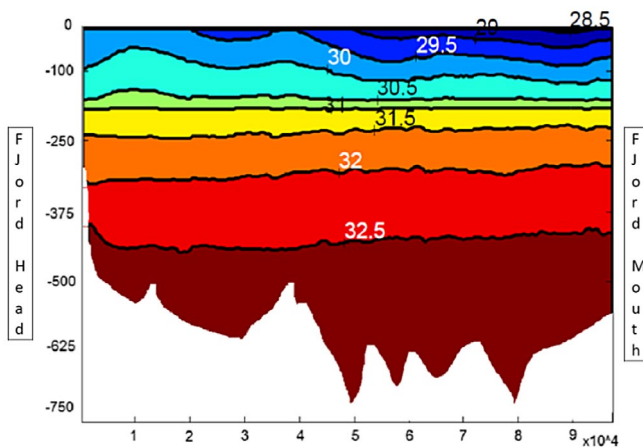
Figure 17. Longitudinal cross section of the salinity profile at the end of the tidal simulation.

4. Conclusions

The temperature and salinity profiles in the model domain are sensitive to the choice of the temperature and salinity values at the open boundary. In order to decrease the open boundary influence on the whole fjord dynamics, the open boundary has been pushed back as far as 50 km away from the fjord entrance. After a number of tests and calibration processes, taking into consideration the model size, the combination of choices for diffusion and advection schemes produced good results for the numerical mixing with a stable stratification. With application of additional forces: wind, Coriolis and tides, the stratification has been broken through the whole water column.

TELEMAC-3D is a suitable model to simulate accurately such a complicated dynamic as in the presented case study. With the help of the numerical model application and various MATLAB tools the major conclusions of this work can be summarised as follows:

(1)   The presented choice of the model grid, schemes, and model parameters produced a stable stratification in the fjord with accurate validation results.

(2)   It has been shown that the *winter* wind scenario drives much stronger circulation at the surface than the *summer* winds. The results show the difference by as much as 0.8 m/s at the middle of the fjord. As a result of the wind activities, the higher the velocities of the flow, the more water mass is delivered to the front of the glacier in an upper part of the water column, and that might have an effect on the ice melt rate, especially when upwelling, at the head of the fjord, is present.

(3)   As a result of the wind forcing on the fjord, the correlation between wind speed and the surface velocities is of great importance. It was shown that the wind speed, with its fluctuations, has a direct and instant impact on the fjord surface velocities.

(4)   It can be concluded that due to the Ekman transport, which can produce *emptying* or *flooding* of the fjord, the wind directions set the surface elevation, upwelling or downwelling events.

(5)   The output of the tidal amplitude of the model simulation matches the measured tidal amplitude accurately with RMSE = 0.05. The results were taken from the point far away from the open boundary in a much shallower region, and good validation results show that the model simulates the tidal propagation in the fjord with a high accuracy level.

(6)   Due to the sharp changes in the fjord width at the entrance and with the addition of the Coriolis force, the fastest residual velocities were observed at the eastern side of the fjord entrance.

(7)   It has been shown that tidal propagation has an effect on the stratification with salinity picks being 5–6 h behind the tidal flood and ebb picks.

Earlier work has shown that wind forcing is a major driver for the fjord circulation. Our research shows this is the case, but that tidal forcing can be as important as wind, as a mixing force, especially in summer time when the wind speeds are much lower. Both of these factors are very important and need to be included in fjord modelling. Further work is underway to recreate a more 'realistic scenario', that includes the under glacier water discharge. This plays a big role in fjord circulation dynamics (Cottier et al., 2010; Murray et al., 2010; Straneo et al., 2010), especially in summer time, when the ice melting rate is at its highest. The analysis of the final 'realistic scenario' results will help us to understand the dynamics of the complicated fjord system, what affect it has on the shrinking Greenland Ice Sheet, and as a result of this, the global sea level rise and what future it brings to us.

ORCID

Violeta Moloney http://orcid.org/0000-0001-6697-0526
Alistair Everett http://orcid.org/0000-0002-4045-4491

References

Buch, E. (2002). Present oceanographic conditions in Greenland waters. *Danish Meteorological Institute Scientific Report, 02–02*, 1–39.

Burchard, H., & Rennau, H. (2007). Comparative quantification of physically and numerically induced mixing in ocean models. *Ocean Modelling, 20*, 293–311.

Cottier, F. R., Nilsen, F., Skogseth, R., Tverberg, V., Skardhamar, J., & Svendsen, H. (2010). Arctic fjord: A review of the oceanographic environment and dominant physical processes. *Geological Society, 344*, 35–50.

Egbert, G. D., & Erofeeva, S. Y. (2002). Efficient inverse modeling of barotropic ocean tides. *Journal of Atmospheric and Oceanic Technology, 19*, 183–204. doi: http://dx.doi.org/10.1175/1520-0426(2002)019<0183:EIMOBO>2.0.CO;2.

Hervouet, J.-M. (2007). *Hydrodynamics of free-surface flows modelling with the FEM*. Chichester: Wiley.

Jackson, R. H., Straneo, F., & Sutherland, D. A. (2014). Externally forced fluctuations in ocean temperature at Greenland glaciers in non-summer months. *Nature Geoscience, 7*, 503–508.

Klinck, J. M., O'Brien, J. J., & Svendsen, H. (1981). A simple model of fjord and coastal circulation interaction. *Journal of Physical Oceanography, 11*, 1612–1626.

Mamayev, O. I. (1975). *Temperature-Salinity analysis of world ocean waters*. Amsterdam: Elsevier.

McPhee, M. G., Skogseth, R., Nilsen, F., & Smedsrud, L. H. (2013). Creation and tidal advection of a cold salinity front in Storfjorden: 2. Supercooling induced by turbulent mixing of cold water. *Journal of Geophysical Research: Oceans, 118*, 3737–3751.

Murray, T., Scharrer, K., James, T. D., Dye, S. R., Hanna, E., Booth, A. D., … Huybrechts, P. (2010). Ocean regulation hypothesis for glacier dynamics in southeast Greenland and implications for ice sheet mass changes (pp. 1–15). *Journal of Geophysical Research, 115*, F03026.

Parker, B. B. (2007). *Tidal analysis and prediction*. Maryland: NOAA Special Publication NOS -OPS 3.

Pawlowicz, R., Beardsley, B., & Lentz, S. (2002). Classical tidal harmonic analysis including error estimates in MATLAB using T TIDE. *Computers & Geosciences, 28*, 929–937.

Riemenschneider, U., & Legg, S. (2007). Regional simulations of the Faroe Bank Channel overflow in a level model. *Ocean Modelling, 17*, 93–122.

Schureman, P. (1941). *Manual of harmonic analysis and prediction of tides*. Washington, WA: Government Printing Office.

Sciascia, R., Cenedese, C., Nicoli, D., Heimbach, P., & Straneo, F. (2014). Impact of periodic intermediary flows on submarine melting of a Greenland glacier. *Journal of Geophysical Research: Oceans, 119*, 7078–7098.

Straneo, F., Hamilton, G. S., Sutherland, D. A., Stearns, L. A., Davidson, F., Hammill, M. O., … Rosing-Asvid, A. (2010). Rapid circulation of warm subtropical waters in a major glacial fjord in East Greenland. *Nature Geoscience, 3*, 182–186.

Sutherland, D. A., Straneo, F., & Pickart, R. S. (2014). Characteristics and dynamics of two major Greenland glacial fjords. *Journal of Geophysical Research: Oceans, 119*, 3767–3791.

Van As, D., Fausto, R. S., Steffen, K., & PROMICE project team. (2014). Katabatic winds and piteraq storms: Observations from the Greenland ice sheet. *Geological Survey of Denmark Greenland Bullrtin, 31*, 83–86.

Wells, N. (1986). *The atmosphere and ocean: A physical introduction*. Chichester: Viley-Blackwell.